ELSEVIER

Earth and Planetary Science Letters 175 (2000) 145–160

EPSL

www.elsevier.com/locate/epsl

Geomagnetic paleointensity for the last 100 kyr from the sub-antarctic South Atlantic: a tool for inter-hemispheric correlation

J.E.T. Channell [a,*], J.S. Stoner [b], D.A. Hodell [a], C.D. Charles [c]

[a] *Department of Geological Sciences, University of Florida, Gainesville, FL 32611-2120, USA*
[b] *Department of Geology, University of California, Davis, CA 95616, USA*
[c] *Scripps Institution of Oceanography, La Jolla, CA 92093-0220, USA*

Received 26 July 1999; accepted 10 November 1999

Abstract

We report relative paleointensity proxy records from four piston cores collected near the Agulhas Ridge and Meteor Rise (South Atlantic). The mean sedimentation rate of the cores varies from 24 cm/kyr to 11 cm/kyr. The two cores with mean sedimentation rates over 20 cm/kyr record positive remanence inclinations at 40–41 ka coeval with the Laschamp Event. Age models are based on oxygen isotope data from three of the cores, augmented by radiocarbon ages from nearby Core RC11-83, and by correlation of paleointensity records for the one core with no oxygen isotope data. The relative paleointensity proxy records are the first from the South Atlantic and from the high to mid-latitude southern hemisphere. Prominent paleointensity lows at ~40 ka and ~65 ka, as well as many other features, can be correlated to paleointensity records of comparable resolution from the northern hemisphere. The records are attributable, in large part, to the global-scale field, and therefore have potential for inter-hemispheric correlation at a resolution difficult to achieve with isotope data alone.

Keywords: paleomagnetism; secular variations; correlation; South Atlantic

1. Introduction

The millennial-scale correlation of climate records of the last glacial cycle from the northern and southern hemisphere is a high priority for understanding inter-hemispheric phase relationships and global climate forcing. Identifying the driving forces for Dansgaard–Oeschger events, for example, requires the ability to construct a detailed sequence of events in the global ocean over a total span of less than a few thousand years. This requirement establishes an immediate need for a globally applicable correlation tool that has sufficient structure on millennial time-scales.

The longer wavelength (~10^4–10^5 year) features in sedimentary relative paleointensity records can be correlated over many thousands of km, from the North Atlantic Ocean to the Mediterranean Sea, and to the Northern Indian and Pacific oceans [1–11]. The few high resolution

* Corresponding author. Tel.: +1-352-392-3658; Fax: +1-352-392-9294; E-mail: jetc@nersp.nerdc.ufl.edu

0012-821X/00/$ – see front matter
PII: S0012-821X(99)00285-X

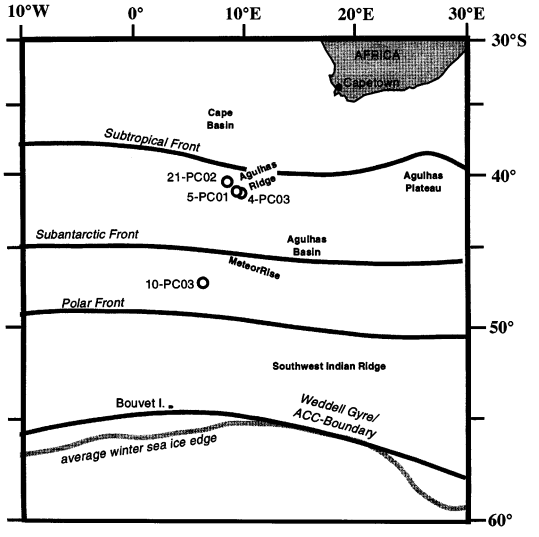

Fig. 1. Location map for piston Cores 21-PC02, 5-PC01, 4-PC03 and 10-PC03.

paleointensity records that are available (e.g. [1,2,5,10]) indicate that the records may correlate at millennial-scale over large distances; however, this is difficult to establish unequivocally because of the limited resolution of oxygen isotope stratigraphy. Up to now, no paleointensity records have been available from the high or mid-latitude southern hemisphere to test whether the observed paleointensity variations are attributable to the global-scale geomagnetic field.

Here, we report data from a suite of upper Quaternary piston cores from the sub-antarctic SE Atlantic Ocean (off South Africa) collected by the R/V *Thompson* in February–March 1996 during a site survey cruise (TTN-057) for ODP Leg 177. The coring targets included sites with sedimentation rates in excess of 10 cm/kyr, designed to provide high resolution climate records in cores with sufficient calcium carbonate for carbon/oxygen isotopic studies. Four piston cores (Fig. 1, Table 1) have been chosen based on their sedimentation rates, apparent continuity of sedimentation (i.e. no turbidites), lithology and shipboard multi-sensor track profiles. Lithologies range from calcareous to siliceous mud and ooze (Table 1). Three of the cores are from north of the Polar Front Zone, thereby avoiding potential sampling problems associated with high diatom concentrations south of the Polar Frontal Zone. The most southern core (10-PC03) was located south of the Polar Front during glacial intervals.

Archive halves of core sections (stored at Lamont–Doherty Earth Observatory) were sampled using plastic u-channels [12] with a 2×2 cm square cross-section and a lid constituting one of the sides. An empty u-channel (without lid), of the same length as the core section, was pushed into the split face of the core section (usually 1.5 m length) until the u-channel filled with sediment. The sediment at the base of the u-channel was then cut away with fishing line, the u-channel extracted, and the lid clipped in place. The ends of the u-channel were sealed with plastic end-pieces and clear polyethylene tape. U-channels were refrigerated at 6°C during storage at the University of Florida, and measured after warming to room temperature. The working halves of three cores (21-PC02, 5-PC01 and 10-PC03) were sampled at 2–5 cm intervals for oxygen and carbon isotope analyses, and percent carbonate analyses.

Table 1
Core studies from cruise TTN-057

Core	Length (m) Water depth (m)	Lat S. Long E.	Nearest ODP/Vema station (ODP site)	Location	Lithology	Sed. rate
4-PC03	11.62	40°56.04	SubSAT-1	N. Agulhas Ridge	Muddy/calcareous	24.4 cm/kyr
	4622	9°53.65	(Site 1089)			
5-PC01	12.65	41°00.03	SubSAT-1	N. Agulhas Ridge	Muddy/calcareous	20.5 cm/kyr
	4702	9°39.74	(Site 1089)			
21-PC02	13.95	41°08.41	V14-65	N. Agulhas Ridge	Muddy/calcareous	13.5 cm/kyr
	4977	7°48.46	(Site 1089)			
10-PC03	11.44	47°05.81	TSO-5	W. Meteor Rise	Muddy/siliceous	11.3 cm/kyr
	4109	5°54.97	(Site 1091)			

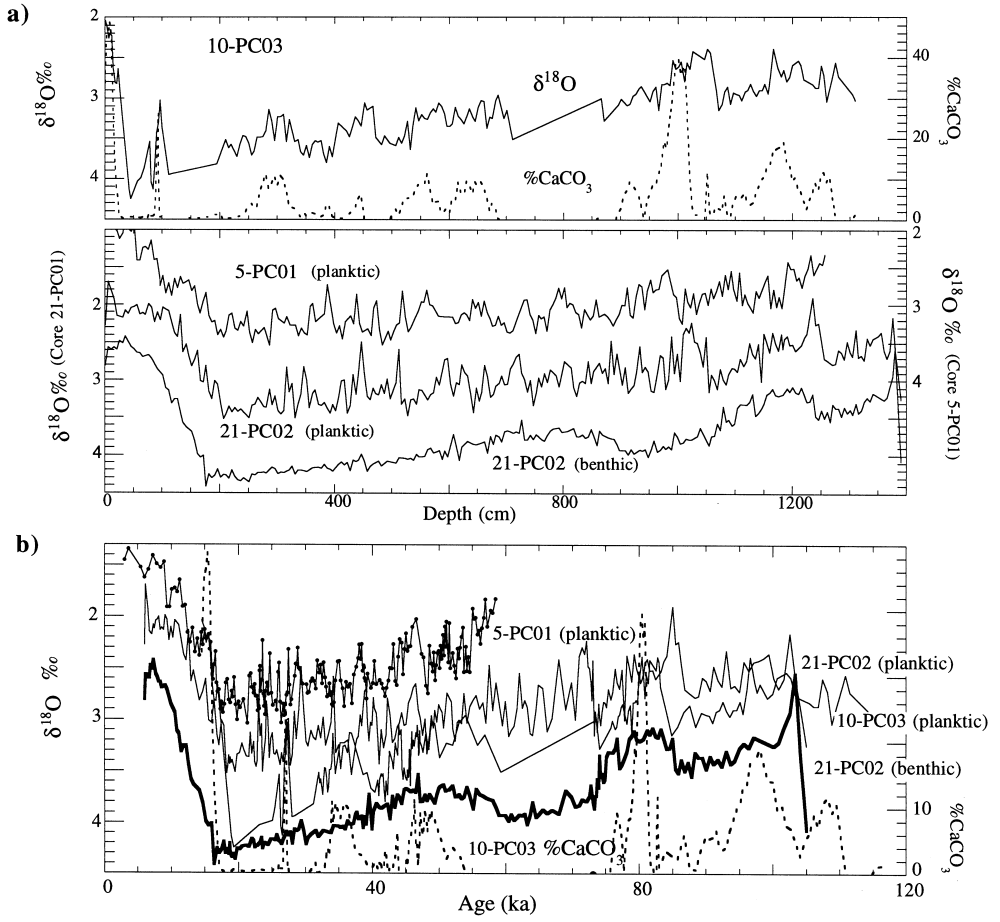

Fig. 2. (a) Oxygen isotope and percent carbonate data for Cores 5-PC01, 10-PC03 and 21-PC02 plotted against depth in core. For Core 10-PC03, the planktic $\delta^{18}O$ data (*N. pachyderma* sinistral) are shown with percent carbonate. For Cores 5-PC01 and 21-PC02, the planktic (*G. bulloides*) and benthic data (*C. wuellerstorfi*) are labeled. (b) The $\delta^{18}O$ and percent carbonate data plotted on their respective age models.

2. Lithology and age models

Planktic oxygen isotope measurements were carried out on monospecific samples of *Globigerina bulloides* selected from the 212–300 μm size fraction in Cores 5-PC01 and 21-PC02, and *Neogloboquadrina pachyderma* (sinistral) from the >150 μm fraction in Core 10-PC03. For benthic foraminifera, we used specimens of *Cibicidoides wuellerstorfi* and *C. kullenbergi* selected from the >150 μm size fraction in Cores 5-PC01 and 21-PC02 (see [13,14]). Samples were reacted in a common acid bath of orthophosphoric acid at 90°C using a VG Isocarb preparation system (Core 10-PC03) or a Carousel-48 automatic carbonate device (Cores 5-PC01 and 21-PC02). Isotopic ratios of purified CO_2 gas were measured on-line with a VG Prism series II mass spectrometer at the University of Florida (Core 10-PC03), and with a Finnigan MAT 252 at Scripps Institution of Oceanography (Cores 5-PC01 and 21-PC02). Analytical precision is better than ±0.1% for $\delta^{18}O$ in both laboratories. Weight percent carbonate for Core 10-PC03 was determined by coulometric titration with an estimated precision of ±1%.

Core 21-PC02 has uniform lithology comprising light gray to gray ooze with varying amounts of calcareous and siliceous components. The top 70 cm has a light yellowish-brown color associated with oxidizing conditions at the sediment-water interface. The 14 m core was recovered in excellent condition with no evidence of coring deformation. To develop the chronology for Core 21-PC02, the planktic and benthic carbon and oxygen isotope data (Fig. 2) were matched to those from nearby Core RC11-83 (41°36'S, 9°48'E) [15]. RC11-83 has 14 radiocarbon ages in the 11–41 ka interval and an identified stage 4/3 oxygen isotope boundary. The chronology obtained by correlation to RC11-83 is supported by the agreement between the 21-PC02 benthic $\delta^{18}O$ record (Fig. 2) and the SPECMAP reference curve [16].

Core 5-PC01 comprises light gray calcareous ooze with a 23 cm oxidized surface layer. Following the methodology used for Core 21-PC02, the chronology for Core 5-PC01 was determined by matching the planktic $\delta^{18}O$ record (Fig. 2) and $\delta^{13}C$ record to those from Core RC11-83 [15] and thereby utilizing the AMS ^{14}C chronology from Core RC11-83.

Core 10-PC03 comprises light gray diatomaceous ooze with calcareous interbeds. The site is located on the western side of the Meteor Rise (Fig. 1, Table 1) and is the most southern of the cores discussed here. Diatoms dominate the biogenic component during glacials and carbonate dominates during interglacials. The uppermost 25 cm comprises a very pale brown oxidized surface layer, and the uppermost 40 cm shows coring-related disturbance. Carbonate analyses show that the core is devoid of carbonate in the glacial intervals (Fig. 2). The lack of carbonate in these intervals limits the resolution of the oxygen isotope stratigraphy. The chronology for 10-PC03 is based on correlation of the planktic $\delta^{18}O$ to the planktic and benthic $\delta^{18}O$ records from Core 21-PC02, augmented by the correlation of intervals devoid of carbonate (Fig. 2) to isotopic stages 2 and 4. Within these constraints, the age model for Core 10-PC03 is then adjusted by matching the paleointensity record to that of Core 21-PC02, and utilizing the 21-PC02 chronology.

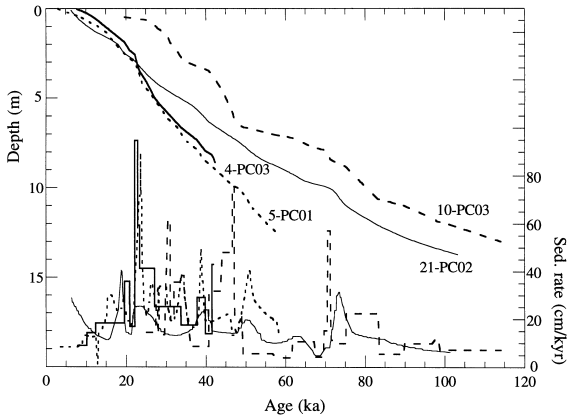

Fig. 3. Depth–age plot for the studied cores, indicating interval sedimentation rates.

Core 4-PC03 comprises uniform light gray calcareous ooze (Table 1). As there are no isotope data for Core 4-PC03, age control was determined by matching paleointensity data to that from 21-PC02, thereby transferring the 21-PC02 chronology to this core.

The resulting age models yield mean sedimentation rates in the 11–24 cm/kyr range. Interval sedimentation rates vary from a few cm/kyr to ~90 cm/kyr (Fig. 3). Cores for which the chronology was deduced by matching to Core RC11-83 (Cores 5-PC01 and 21-PC02) show smoother variations in sedimentation rates than the abrupt square-wave pattern deduced from matching paleointensity data (Cores 10-PC03 and 4-PC03). This is a result of the relatively small number of tie-points used in the paleointensity match. Sedimentation rates greater than 40 cm/kyr apparently occur at 22–25 ka in Cores 5PC01 and 4-PC03, at ~38 ka in Core 5-PC01, and at ~31 ka, ~47 ka and ~71 ka in Core 10-PC03 (Fig. 3).

3. Magnetic properties

Magnetic measurements were carried out at 1 cm or 2 cm intervals on an automated 2G 'u-channel' cryogenic magnetometer [17] at the University of Florida. Prior to the arrival of the u-channel magnetometer in Florida (March 1998), initial measurements for two cores were carried

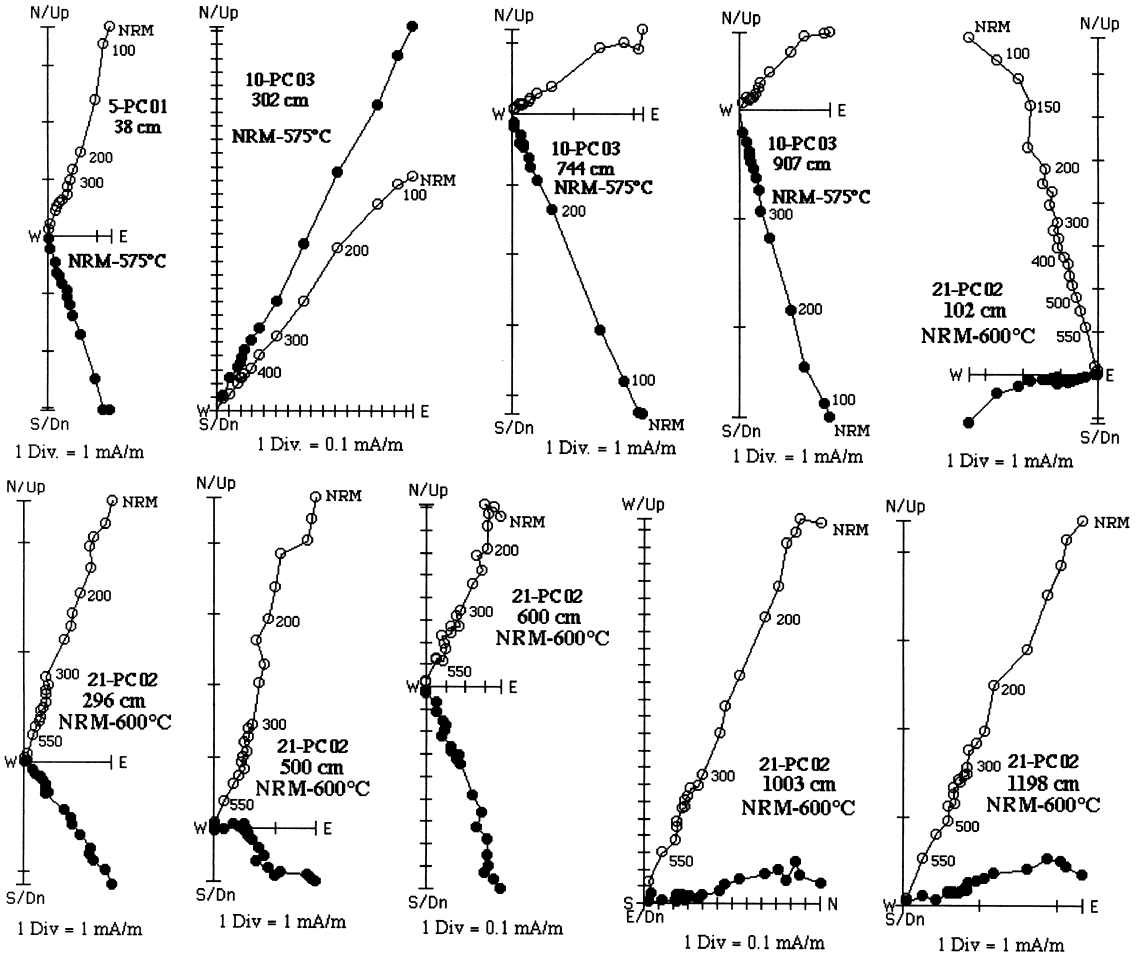

Fig. 4. Orthogonal projections of thermal demagnetization data. Open and closed symbols represent projection of the vector endpoints on the vertical and horizontal planes, respectively. The temperature associated with certain points is indicated in °C. The depth in the core of each sample is indicated.

out by Y. Guyodo at IPG (Paris). The standard u-channel remanence measurement procedure comprised stepwise alternating field (AF) demagnetization of natural remanent magnetization (NRM) in 5 mT steps from 10 to 50 mT and then 10 mT steps to 100 mT. The anhysteretic remanent magnetization (ARM) was then acquired in a 100 mT AF and a 0.05 mT biasing field. The ARM was then stepwise demagnetized in the same peak fields as applied to the NRM. Finally, the isothermal remanent magnetization (IRM) was then acquired in a 1 T field, then demagnetized in the same peak fields as applied to the NRM and ARM. Discrete 7 cm^3 cubic samples were used to determine the blocking temperature spectrum of the NRM, and to resolve magnetization components for comparison with u-channel measurements of an apparent magnetic excursion. Subsamples from these cubes were used to measure hysteresis parameters.

Thermal demagnetization of NRM indicates unblocking temperatures below 600°C for all cores (Fig. 4). Substantial unblocking of NRM in the 500–575°C temperature interval, particularly in Core 21-PC02, is indicative of a magnetite remanence carrier. The lack of unblocking above

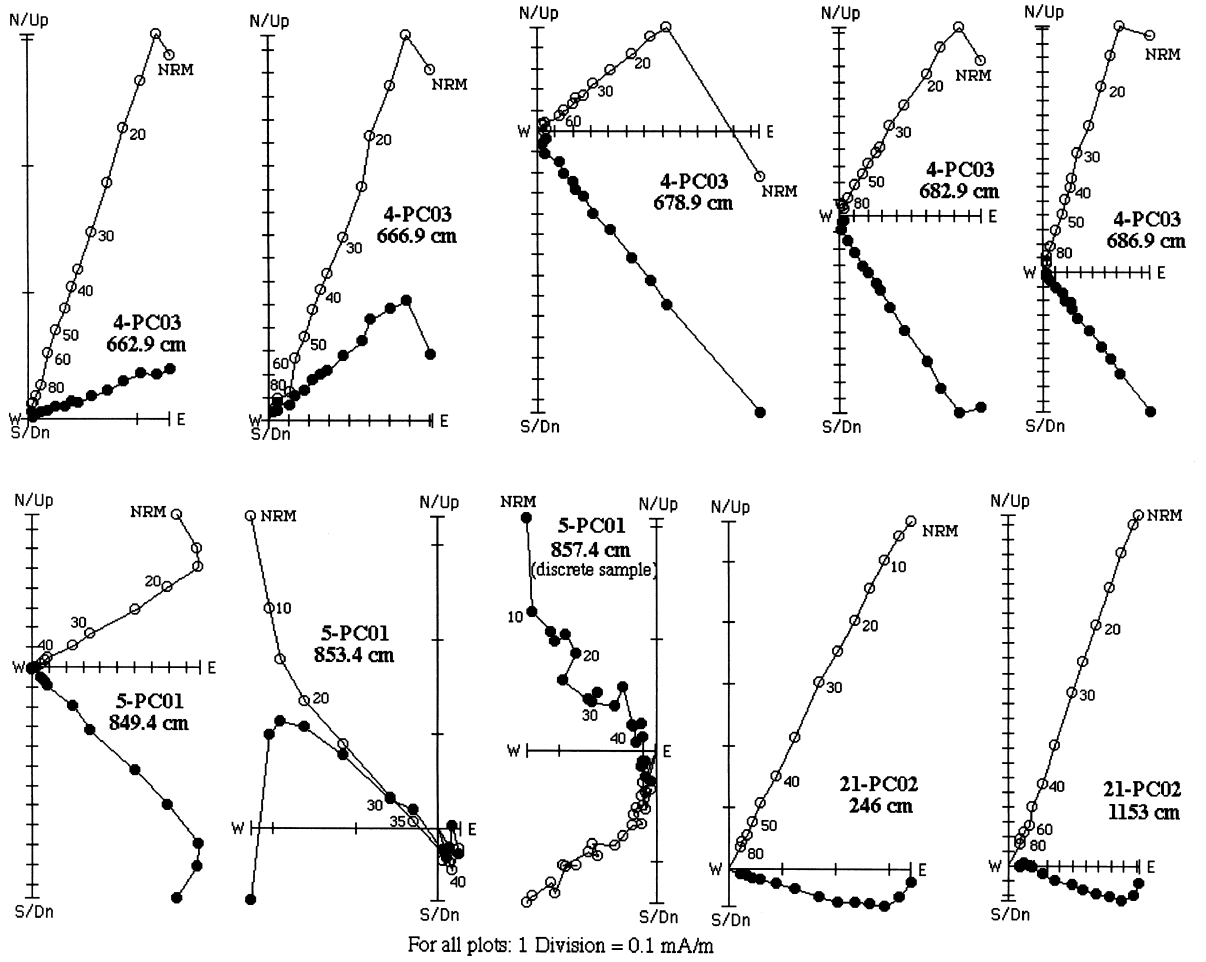

Fig. 5. Orthogonal projections of AF demagnetization data. Open and closed symbols represent projection of the vector endpoints on the vertical and horizontal planes, respectively. The peak fields associated with certain points are indicated in mT. The depth in the core of each sample is indicated.

600°C tends to indicate that hematite is not an important contributor to the NRM. AF demagnetization of NRM indicates that the NRM has fairly high coercivities (Fig. 5). The median destructive field of NRM lies in the 20–40 mT range and a small proportion ($<10\%$) of NRM intensity remains after demagnetization in peak AFs of 80 mT.

Hysteresis ratios appear to lie on a magnetite grain size mixing line within the pseudo-single domain (PSD) field (Fig. 6a). Values from the base of the two cores (particularly sample 1299.70 cm from close to the base of 10-PC03) are displaced to higher values of Hcr/Hc (Fig. 6a). For these samples, the hysteresis loops are slightly wasp-waisted and the saturation fields are raised from about 0.1 T to about 0.4 T, indicating the presence of a high coercivity mineral coexisting with magnetite. Thermal demagnetization of NRM (Fig. 4) shows no evidence for a contribution from minerals other than magnetite (e.g. hematite or pyrrhotite), however, thermal demagnetization of a three-axis IRM indicates a concentration of unblocking temperatures below

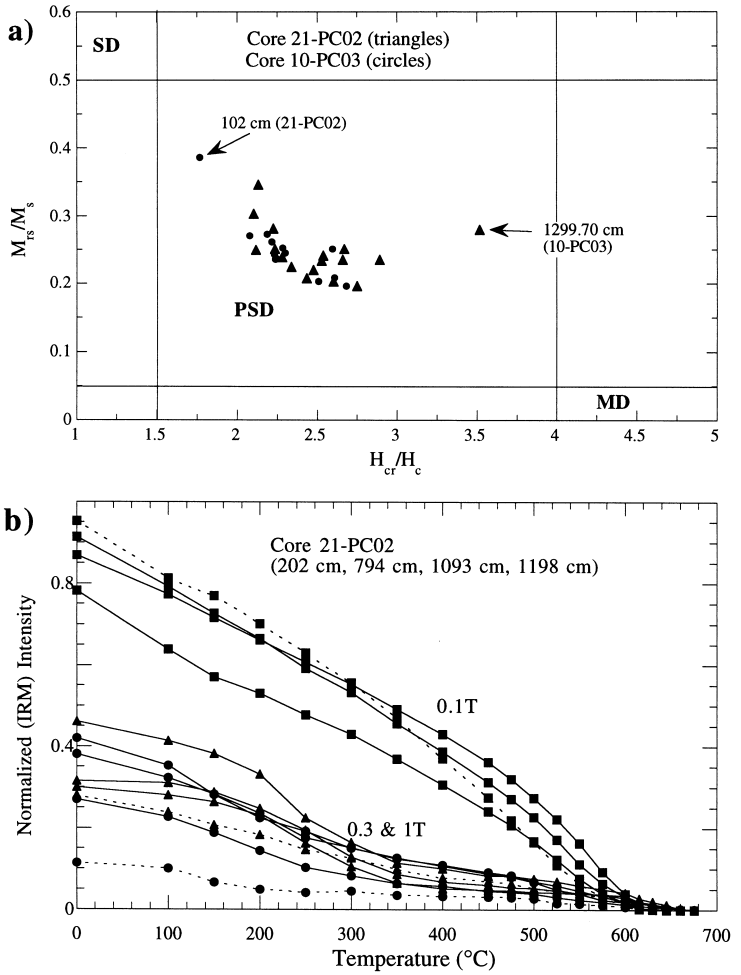

Fig. 6. (a) Hysteresis ratio plot for samples from Cores 21-PC02 (closed circles) and 10-PC03 (triangles). SD, PSD and multidomain (MD) fields after [33]. (b) Thermal demagnetization of a three-axis composite IRM for four samples from Core 21-PC02. Orthogonal DC fields of 1 T (circles), 0.3 T (triangles) and 0.1 T (squares) were applied sequentially to each sample prior to heating [34]. The 0.1 T IRM is dominated by unblocking temperatures distributed below 600°C whereas the 0.3 and 1 T IRMs appear to include a concentration of unblocking below about 350°C. Dashed line indicates the shallowest sample at 202 cm depth.

350°C for some samples (Fig. 6b), particularly those from close to the base of cores, implying the presence of (diagenetically produced) iron sulfides.

The plot of anhysteretic susceptibility (κ_{arm}) against susceptibility (κ) has been used as a means of estimating magnetite grain size in sediments [18,19]. According to the calibration of [18], the magnetite grain size lies close to 5 μm for the last glacial interval (isotopic stages 2–4), and is finer during the Holocene and stage 5 (Fig. 7). The presence of finer grain sizes during interglacials may be attributed to enhanced production of fine (possibly biogenic) magnetite, or to enhanced preservation of fine magnetite particles. The hysteresis ratios for the one sample from the Holocene of Core 21-PC02 (102 cm) lies towards the single domain (SD) field in the hysteresis ratio plot (Fig. 6a). Volume susceptibility varies by a factor of 4–5 downcore. IRM tends to mimic sus-

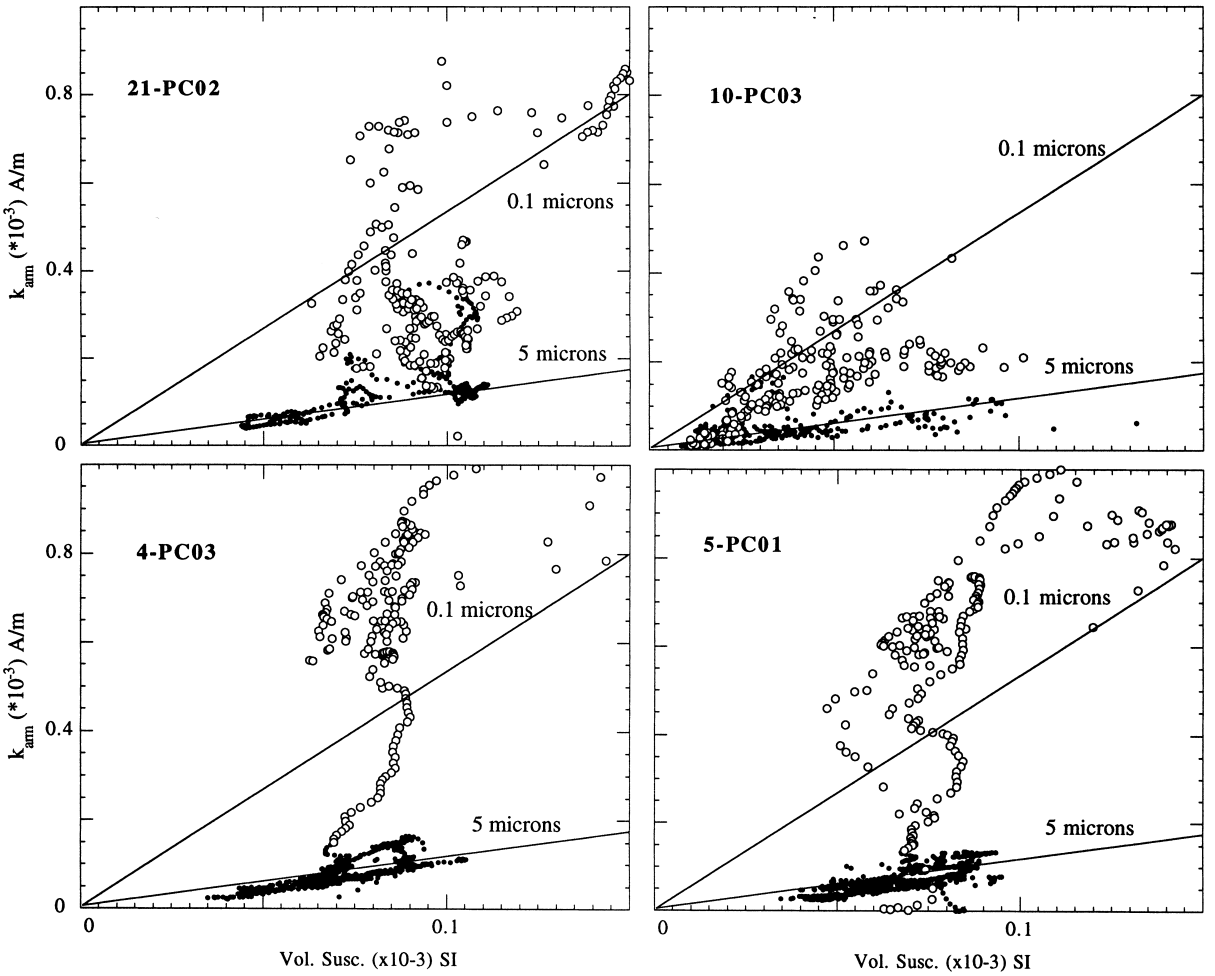

Fig. 7. Anhysteretic susceptibility (κ_{arm}) plotted against susceptibility (κ). For Cores 4-PC03 and 5-PC01, open symbols indicate Holocene samples. For 21-PC02 and 10-PC03, open symbols indicate Holocene and isotopic substage 5a samples. The lines corresponding to a magnetite grain size of 0.1 μm and 5 μm are shown (after [18]).

ceptibility with variations downcore by a factor of about 6–8. Well-defined magnetization components carried by magnetite (Figs. 4 and 5), PSD grain size in magnetite (Fig. 6), and variation in the magnetic concentration parameters, by a factor less than 10, are among the proposed criteria for paleointensity studies [18,19].

4. NRM directions

NRM component directions were calculated (at 1 cm intervals) using the standard least squares method [20] applied to the 20–80 mT demagnetization interval. Component inclinations, placed on individual age models, are shown in Figs. 8 and 9. For Cores 21-PC02, 4-PC03 and 5-PC01, maximum angular deviation (MAD) values are generally below 10°, indicating that the magnetization components are well-defined. The inclination varies about mean values close to the expected inclination (−60° to −65°) for the site latitudes (41°S–47°S).

Anomalous (positive) inclination values occur

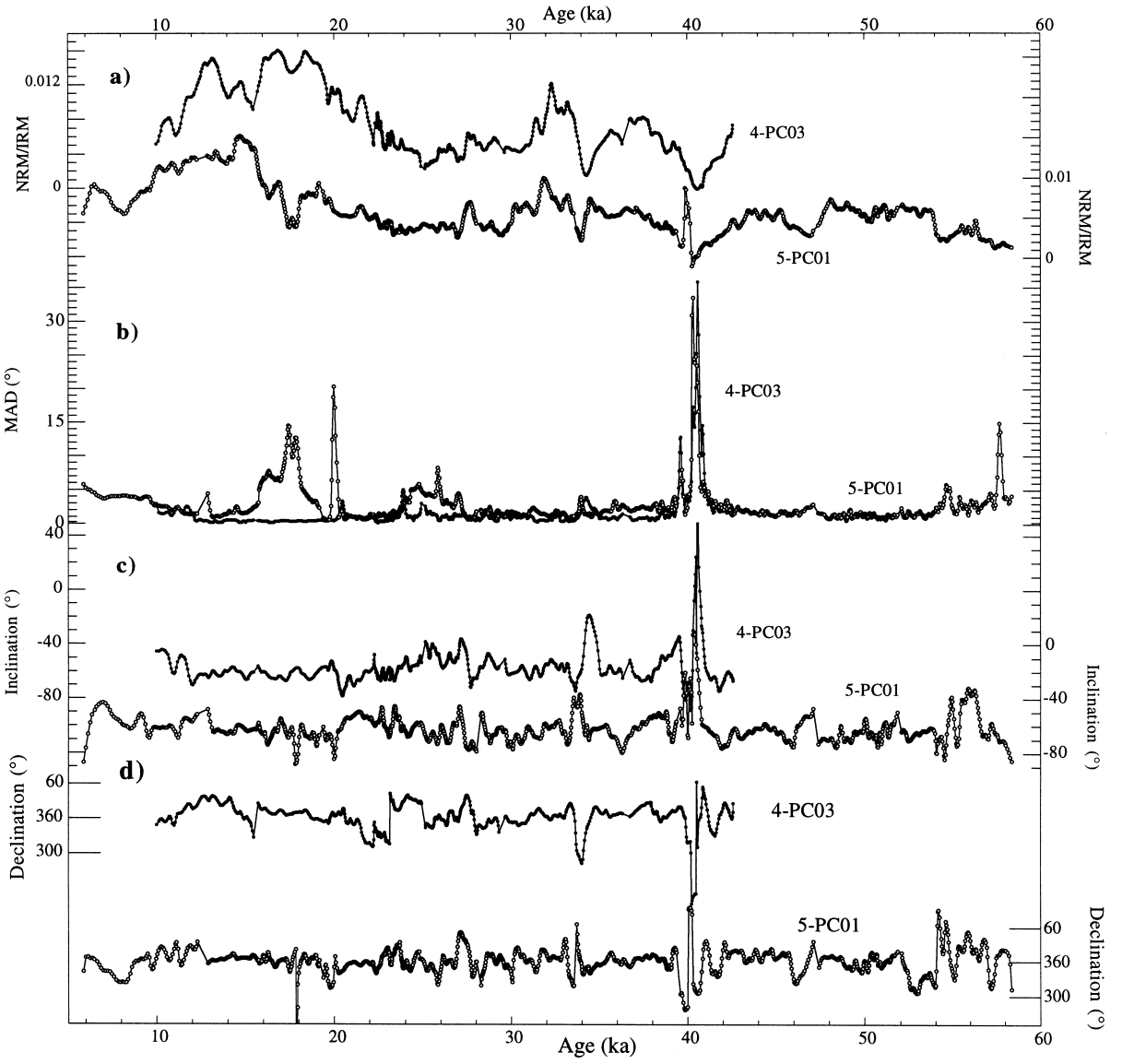

Fig. 8. Cores 4-PC03 and 5-PC01: NRM/IRM (paleointensity proxy), MAD, inclination and declination of the magnetization component computed in the 20–80 mT demagnetization interval.

at about 40 ka in Cores 4-PC03 and 5-PC01 (Fig. 8), and inclinations become shallow in the same time interval in Cores 21-PC02 and 10-PC03 (Fig. 9). For the ~40 ka interval in Core 4-PC03 and 5-PC01 (Fig. 8), the MAD values reach 30° in large part due to the blanket use of the 20–80 mT demagnetization interval for definition of the magnetization component. Sample 853.4 cm in Core 5-PC01 (see Fig. 5) is from the ~40 ka event and the orthogonal projection of demagnetization data illustrates that the positive inclinations are not resolved at peak demagnetization fields below 40 mT. The anomalous inclinations may correspond to the Laschamp Event which has been widely recognized at ~40 ka in the North Atlantic region.

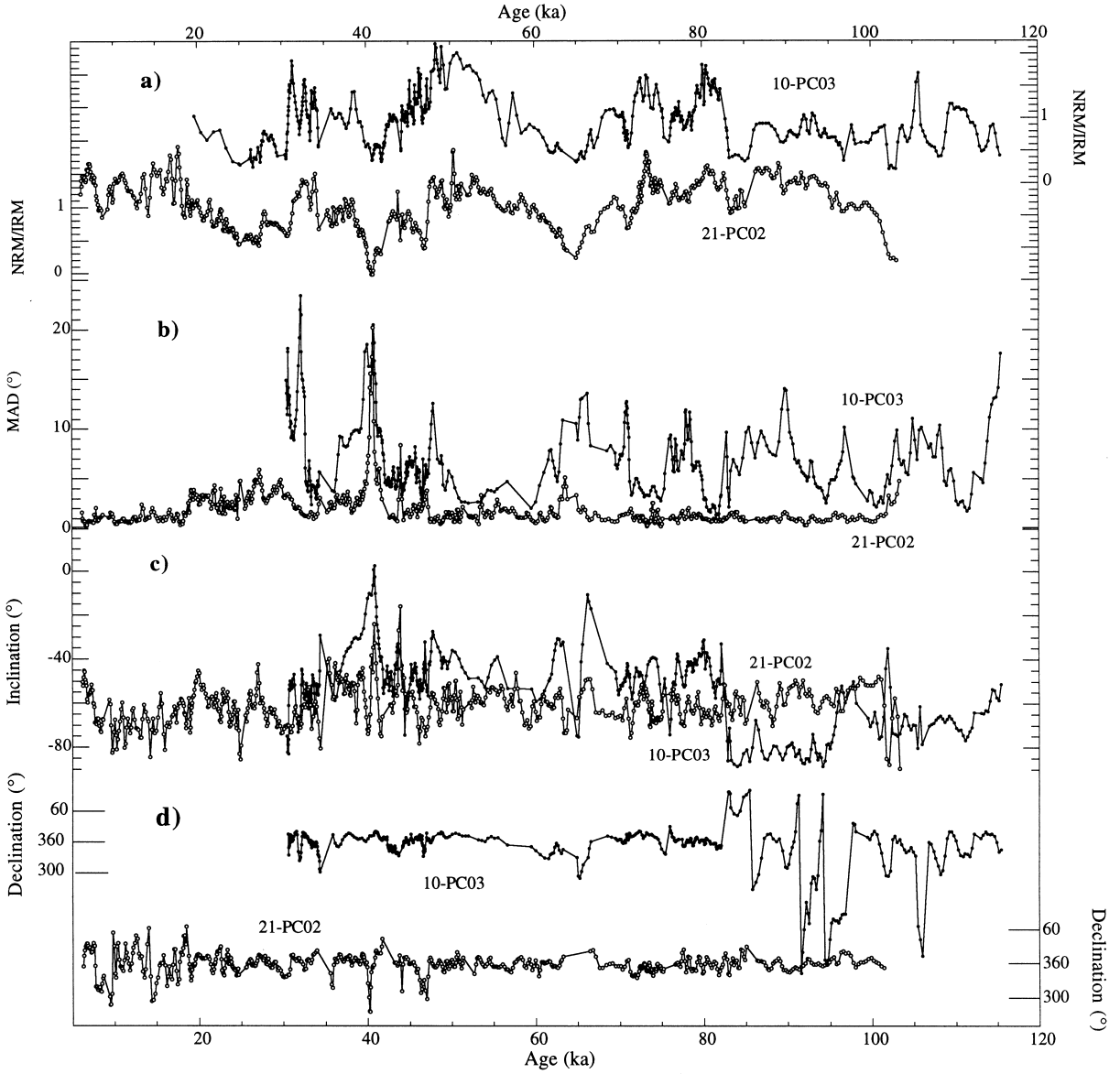

Fig. 9. Cores 10-PC03 and 21-PC02: NRM/IRM (paleointensity proxy), MAD, inclination and declination of the magnetization component computed in the 20–80 mT demagnetization interval.

For Cores 4-PC03 and 5-PC01, discrete 7 cm^3 samples in plastic cubes were collected back-to-back alongside the u-channeled interval recording the anomalous magnetization directions. Stepwise AF demagnetization of the discrete samples (e.g. sample 857.4 cm from Core 5-PC01 in Fig. 5) yielded anomalous magnetization components which are not identical to the components resolved from the u-channel data (Fig. 10) but generally ratify the existence of a directional magnetic excursion. Large swings in declination observed in the u-channel component declinations, but not in the discrete sample data, may be an artifact of u-channel measurements.

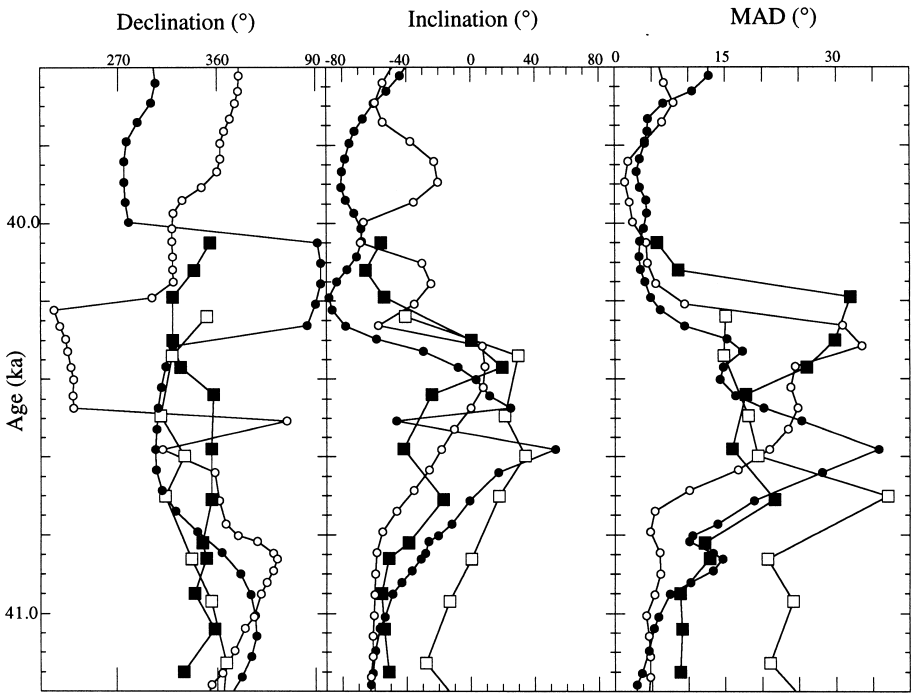

Fig. 10. Component declination and inclination and corresponding MAD values for components computed from u-channel data (circles) and discrete sample data (squares) from Core 5-PC01 (open symbols) and Core 4-PC03 (closed symbols) in the interval recording a magnetic event coeval with the Laschamp Event.

5. Paleointensity determinations

Paleointensity proxies are constructed by normalizing the NRM by an artificial remanence (ARM or IRM) or by susceptibility. The objective is to compensate for changes in concentration of remanence carrying grains. The normalizer should activate the same grain population as that which carries the NRM. In recent studies of North Atlantic sediments (e.g. [10,21,22]), NRM/IRM has been the preferred paleointensity proxy. In these cases, the coercivity spectrum of IRM has been shown to be a closer match (than ARM) to the coercivity spectrum of NRM. This also appears to be the case in the South Atlantic cores discussed here. For example, in Cores 4-PC03 and 5-PC01, the NRM/ARM varies more than NRM/IRM in the 20–60 mT demagnetization range (Fig. 11), indicating that the coercivity of IRM is a closer match to that of NRM in this demagnetization range. For the paleointensity proxy, we determine the subtracted vectors of NRM and IRM in the 30–40 mT demagnetization window, and utilize the subtracted vector NRM/IRM ratio. The use of a particular demagnetization *interval* for calculation of NRM/IRM, rather than a particular demagnetization *value*, is designed to reduce the influence of high coercivity grains on the paleointensity proxy.

The subtracted vector NRM/IRM values are plotted on their respective age models for each core (Figs. 8 and 9). Variations among the records can be attributed to chronological discrepancies, differential diagenesis, vagaries of the recording process and/or lithologic changes not accounted for by the normalization procedure. When comparing the South Atlantic paleointensity signals with records from further afield (e.g. North Atlantic), non-global variability in geomagnetic field strength may also account for the variations in the records. In Fig. 12, we compare the South Atlantic records with two records of similar reso-

lution from the Iceland Basin (North Atlantic) [10,21], Core P-013 from the Labrador Sea and a composite Labrador Sea record [5,22], as well as records from the Mediterranean Sea [1] and Somali Basin [2].

6. Discussion

The interval of positive and shallow inclinations at ~40 ka corresponds to a paleointensity low (Figs. 8 and 9) and is coeval with the Laschamp Event which was originally documented in igneous rocks in France [23]. It has since been found in Icelandic lavas [24,25] and in sediment cores throughout the North Atlantic [26] where the duration of the event has been estimated to be about 1 kyr, similar to that observed here (Fig. 10). Although directional magnetic excursions such as the Laschamp Event are often not recorded, even in high sedimentation rate cores, the paleointensity low of the same age is a resilient feature of paleointensity records (Fig. 12). Directional records of a field excursion may often be lost by overprinting by the stronger post-excursion field [27]. On the other hand, the paleointensity record may be largely controlled by the global-scale (axial dipole) field, whereas the presence or absence of a directional excursion in the record may depend not only on the recording fidelity of the sediment, but also on the presence or absence of a local 'center' of geomagnetic secular variation over the site at the time of a paleointensity low.

Sediment cores with mean accumulation rates of ~10 cm/kyr have yielded relative geomagnetic paleointensity records for the North Atlantic, Labrador Sea, Mediterranean Sea and Somali Basin (Fig. 12). Similarities among these records over the last 200 kyr indicate that the global-scale geomagnetic field has been recorded. Differences among the records can be attributed to lithologic (environmental) variability, stochastic pulses in sedimentation, local (non-global) components of the geomagnetic field and/or chronological discrepancies among the records. The intervals of high κ_{arm}/κ values, generally constrained to the Holocene and isotopic substage 5a (Fig. 7), indicate a high concentration of fine grained magnetite which is probably not adequately normalized by the NRM/IRM ratio.

Inter-hemispheric correlations can be tested by optimally matching the paleointensity records and

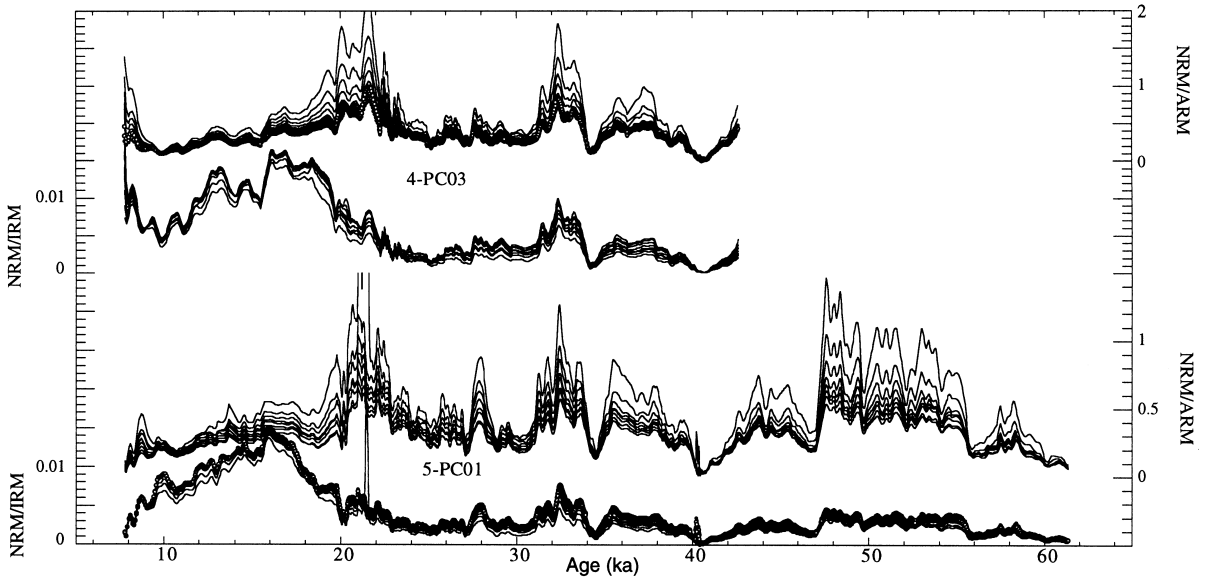

Fig. 11. Cores 4-PC03 and 5-PC01: NRM/ARM and NRM/IRM in the 20–60 mT demagnetization range indicating that the coercivity of IRM is a better match (than ARM) to the coercivity of NRM.

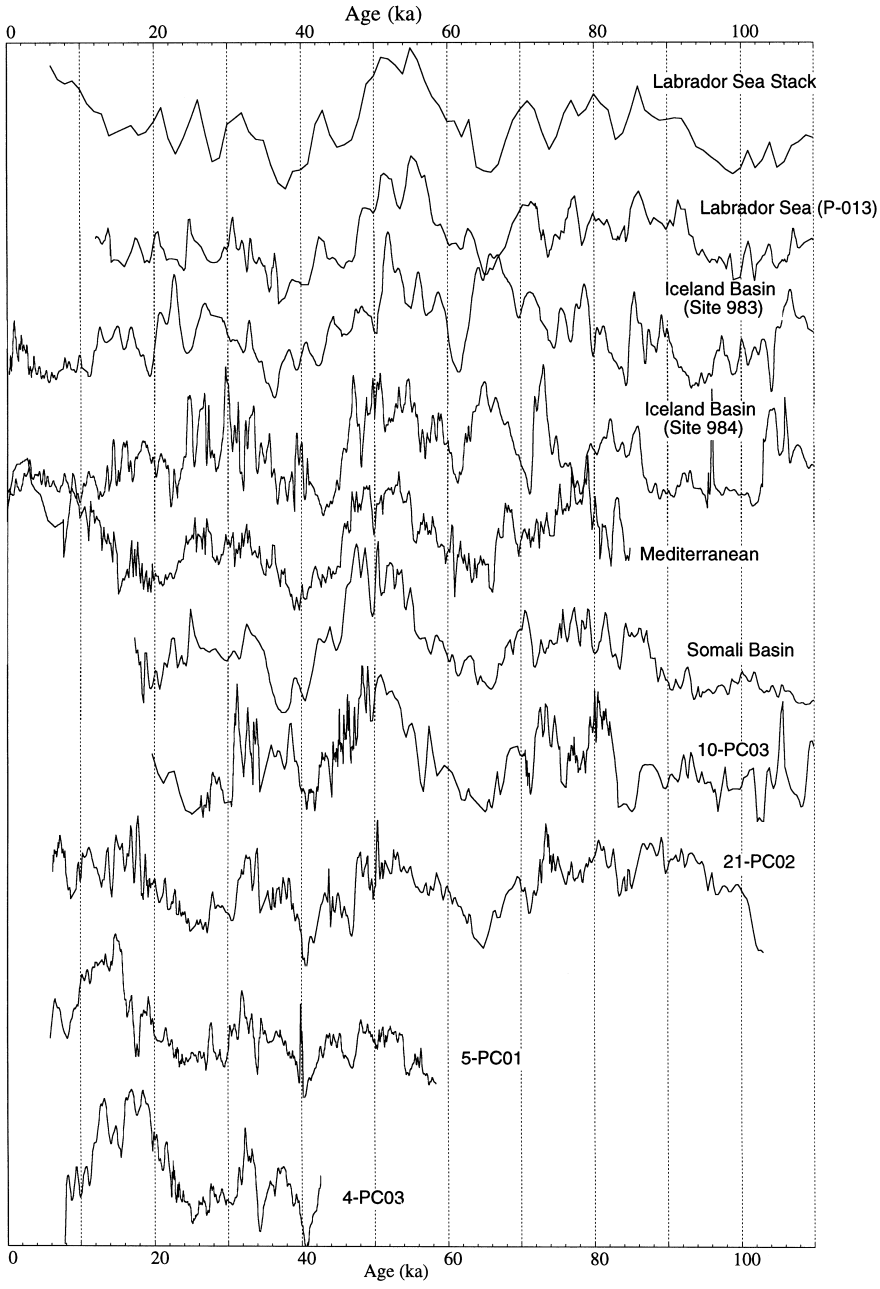

Fig. 12. Comparison of the paleointensity records from the Cores 21-PC02, 10-PC03, 4-PC03 and 5-PC01 with other records of similar resolution. Other records are shown on their individual age models, therefore mismatches in time can be attributed to chronological discrepancies. Records shown: Labrador Sea stack and Core P-013 [5,22], ODP Site 983 and 984 [10,21], Mediterranean record [1], Somali Basin [2].

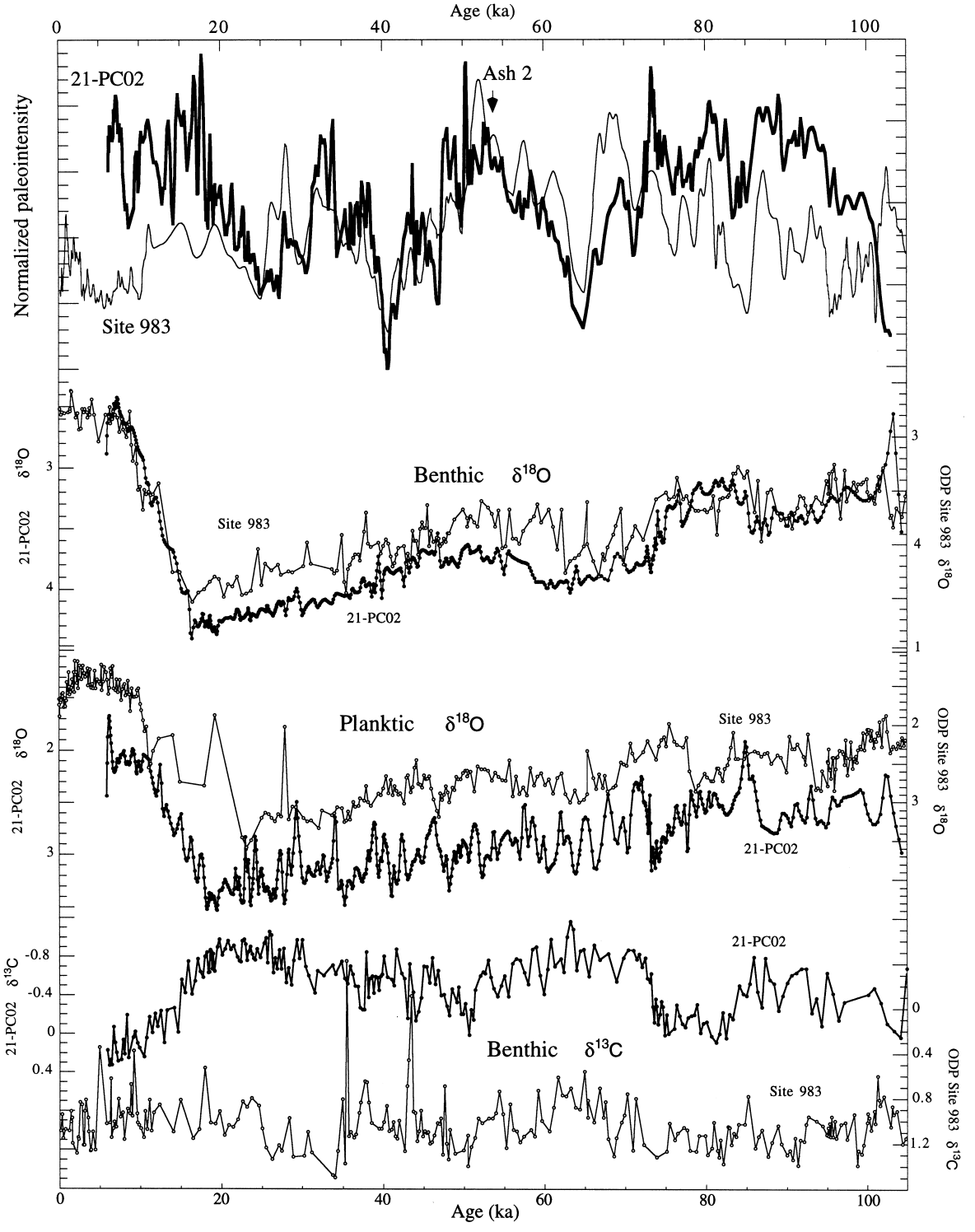
Age (ka)
0
20
40
60
80
100
21-PC02
Ash 2
Site 983
Normalized paleointensity
Benthic δ18O
Site 983
21-PC02
21-PC02 δ18O
ODP Site 983 δ18O
Planktic δ18O
Site 983
21-PC02
21-PC02 δ18O
ODP Site 983 δ18O
21-PC02
Benthic δ13C
Site 983
21-PC02 δ13C
ODP Site 983 δ13C
Age (ka)

Fig. 13. Shape match of Site 983 and Core 21-PC02 paleointensity records (top). Below: Site 983 (open symbols) and Core 21-PC02 (closed symbols) $\delta^{18}O$ and $\delta^{13}C$ records using a common (Core 21-PC02) age model acquired by matching the Site 983 and Core 21-PC03 paleointensity records.
←

determining whether this match violates the benthic $\delta^{18}O$ data, assumed to mainly reflect global ice volume. ODP Site 983 (Iceland Basin) and Core 21-PC02 have high resolution benthic $\delta^{18}O$ records and are therefore suitable for this test. The match based on paleointensity records does not violate the isotopic data from these two cores (Fig. 13). The adjusted Site 983 chronology is consistent with the age for Ash Layer 2 (52 ka) deduced from its identification in the GRIP ice core [28].

The $\delta^{18}O$ of sea water (and $\delta^{18}O$ of atmospheric O_2) is relatively featureless during marine isotopic stages 3 and 4, providing little correlative value during this critical interval. In contrast, the paleointensity record is marked by high amplitude variability during this interval (Fig. 12). As variations in geomagnetic paleointensity control the flux of ^{10}Be and ^{36}Cl isotopes, and these isotopes are readily measurable in ice cores, paleointensity records in marine cores provide an independent link between marine sediment and ice core records [29]. The lows in paleointensity at $\sim$40 ka and $\sim$65 ka (Fig. 12) are readily identifiable as highs in flux of ^{10}Be and ^{36}Cl in the Vostok and Grip ice cores, respectively [30,31]. Frank et al. [32] have shown that 10^4–10^5 year variability in ^{10}Be production rate, as determined from globally distributed deep-sea cores over the last 200 kyr, can be matched to sediment paleointensity data. This observation and the similarity of globally distributed paleointensity records (Fig. 12) indicates that the 10^4–10^5 year variability in paleointensity is globally correlative. The question remains as to whether the 10^3–10^4 year variability recognized in the records (Fig. 12) can be correlated over large distances. Shape match of the paleointensity records from the Site 983 (Iceland Basin) and Core 21-PC02 does not violate the isotopic data (Fig. 13), implying that the 10^3–10^4 year variability may be temporally correlated between the two hemispheres, and is therefore largely attributable to the global-scale field.

Acknowledgements

This research was supported by National Science Foundation (NSF) Grant OCE 97-11424. We thank Y. Guyodo and K. Huang for help with laboratory measurements, J.-P. Valet and T. Yamazaki for reviews of the manuscript, and R. Lotti for assistance with core sampling at the Lamont–Doherty Earth Observatory, where support for the curating facilities is provided by the National Science Foundation and the Office of Naval Research. *[RV]*

References

[1] E. Tric, J.-P. Valet, P. Tucholka, M. Paterne, L. Labeyrie, F. Guichard, L. Tauxe, M. Fontugne, Paleointensity of the geomagnetic field for the last 80 000 years, J. Geophys. Res. 97 (1992) 9337–9351.
[2] L. Meynadier, J.-P. Valet, R. Weeks, N.J. Shackleton, V.L. Hagee, Relative geomagnetic intensity of the field during the last 140 ka, Earth Planet. Sci. Lett. 114 (1992) 39–57.
[3] L. Tauxe, N.J. Shackleton, Relative paleointensity records from Ontong-Java Plateau, Geophys. J. Int. 117 (1994) 769–782.
[4] T. Yamazaki, N. Ioka, Long-term secular variation of the geomagnetic field during the last 200 kyr recorded in sediment cores from the western equatorial Pacific, Earth Planet. Sci. Lett. 128 (1994) 527–544.
[5] J.S. Stoner, J.E.T. Channell, C. Hillaire-Marcel, Late Pleistocene relative geomagnetic paleointensity from the deep Labrador sea: regional and global correlations, Earth Planet. Sci. Lett. 134 (1995) 237–252.
[6] R.C. Weeks, Normalized NRM intensity during the last 240 000 years in piston cores from central North Atlantic Ocean: geomagnetic field intensity or environmental signal?, Phys. Earth Planet. Int. 87 (1995) 213–229.
[7] D.A. Schneider, G.A. Mello, A high-resolution marine sedimentary record of geomagnetic intensity during the Brunhes Chron, Earth Planet. Sci. Lett. 144 (1996) 297–314.
[8] B. Lehman, C. Laj, C. Kissel, A. Mazaud, M. Paterne, L. Labeyrie, Relative changes of the geomagnetic field intensity during the last 280 kyear from piston cores in the Azores area, Phys. Earth Planet. Int. 93 (1996) 269–284.
[9] Y. Guyodo, J.-P. Valet, Relative variations in geomag-

netic intensity from sedimentary records: The past 200 thousand years, Earth Planet. Sci. Lett. 143 (1996) 23–26.
[10] J.E.T. Channell, D.A. Hodell, B. Lehman, Relative geomagnetic paleointensity and $\delta^{18}O$ at ODP Site 983 (Gardar Drift, North Atlantic) since 350 ka, Earth Planet. Sci. Lett. 153 (1997) 103–118.
[11] A.P. Roberts, B. Lehman, R.J. Weeks, K.L. Verosub, C. Laj, Relative paleointensity of the geomagnetic field over the last 200 000 years from ODP Sites 883 and 884, North Pacific Ocean, Earth Planet. Sci. Lett. 152 (1997) 11–23.
[12] L. Tauxe, J.L. LaBrecque, R. Dodson, M. Fuller, U-channels - a new technique for paleomagnetic analysis of hydralic piston cores, Trans. Am. Geophys. Union (EOS) 64 (1983) 219.
[13] D.A. Hodell, C.D. Charles and U.S. Ninnemann, Comparison of interglacial stages in the South Atlantic sector of the Southern Ocean for the past 450 kyrs: implications for Marine Isotope Stage (MIS) 11, Glob. Planet. Chang. (in press).
[14] U.S. Ninnemann, C.D. Charles and D.A. Hodell, Origin of global millennial scale climate events: constraints from the Southern Ocean deep sea sedimentary record, in: Mechanisms of Global Climate Change at Millennial Time Scales, Geophys. Monogr. Ser. 112 (1999) (in press).
[15] C.D. Charles, J. Lynch-Stieglitz, U.S. Ninnemann, R.G. Fairbanks, Climate connections between the hemispheres revealed by deep sea sediment core/ice core correlations, Earth Planet. Sci. Lett. 142 (1996) 19–28.
[16] D.G. Martinson, N.G. Pisias, J.D. Hays, J. Imbrie, T.C. Moore Jr., N.J. Shackleton, Age dating and the orbital theory of the Ice Ages: development of a high-resolution 0 to 300 000-year chronostratigraphy, Quat. Res. 27 (1987) 1–29.
[17] R. Weeks, C. Laj, L. Endignoux, M. Fuller, A. Roberts, R. Manganne, E. Blanchard, W. Goree, Improvements in long-core measurement techniques: applications in palaeomagnetism and palaeoceanography, Geophys. J. Int. 114 (1993) 651–662.
[18] J.W. King, S.K. Banerjee, J. Marvin, A new rock magnetic approach to selecting sediments for geomagnetic intensity studies: application to paleointensity for the last 4000 years, J. Geophys. Res. 88 (1983) 5911–5921.
[19] L. Tauxe, Sedimentary records of relative paleointensity of the geomagnetic field: theory and practice, Rev. Geophys. 31 (1993) 319–354.
[20] J.L. Kirschvink, The least squares lines and plane analysis of paleomagnetic data, Geophys. J. R. Astr. Soc. 62 (1980) 699–718.
[21] J.E.T. Channell, Geomagnetic paleointensity and directional secular variation at Ocean Drilling Program (ODP) Site 984 (Bjorn Drift) since 500 ka: Comparisons with ODP Site 983 (Gardar Drift), J. Geophys. Res. 104 (1999) 22937–22951.
[22] J.S. Stoner, J.E.T. Channell, C. Hillaire-Marcel, A 200 kyr geomagnetic chronostratigraphy for the Labrador Sea: Indirect correlation of the sediment record to SPECMAP, Earth Planet. Sci. Lett. 159 (1998) 165–181.
[23] N. Bonhommet, J. Babkine, Sur la presence d'aimentation inverse dans la Chaine des Puys, C.R. Hebs. Seances Acad. Sci. Ser. B 264 (1967) 92–94.
[24] L. Kristjansson, A. Gudmundsson, Geomagnetic excursion in late glacial basalt outcrops in southwestern Iceland, Geophys. Res. Lett. 7 (1980) 337–340.
[25] S. Levi, H. Gudmunsson, R.A. Duncan, L. Kristjansson, P.V. Gillot, S.P. Jacobsson, Late Pleistocene geomagnetic excursion in Icelandic lavas: confirmation of the Laschamp excursion, Earth Planet. Sci. Lett. 96 (1990) 443–457.
[26] C. Laj, C. Kissel, A. Mazaud, J.E.T. Channell and J. Beer, North Atlantic paleointensity stack since 75 ka (NAPIS-75) and the duration of the Laschamp Event, Trans. R. Soc. Ser. A (2000) (in press).
[27] R.S. Coe, J.C. Liddicoat, Overprinting of a natural magnetic remanence in lake sediments by a subsequent high-intensity field, Nature 367 (1994) 57–59.
[28] K. Grönvold, N. Óskarsson, S. Johnsen, H. Clausen, C. Hammer, G. Bond, E. Bard, Ash layers and Iceland in the Greenland GRIP ice core correlated with oceanic and land sediments, Earth Planet. Sci. Lett. 135 (1995) 149–155.
[29] A. Mazaud, C. Laj, M. Bender, A geomagnetic chronology for antarctic ice accumulation, Geophys. Res. Lett. 21 (1994) 337–340.
[30] S. Baumgartner, J. Beer, J. Masarik, G. Wagner, L. Meynadier, H.-A. Synal, Geomagnetic modulation of the ^{36}Cl flux in the GRIP Ice Core, Greenland, Science 279 (1998) 1330–1332.
[31] G.M. Raisbeck, F. Yiou, D. Bourles, C. Lorius, J. Jouzel, N.I. Barkov, Evidence for two intervals of enhanced ^{10}Be deposition in Antarctic ice during the last glacial period, Nature 326 (1987) 273–277.
[32] M. Frank, B. Schwarz, S. Baumann, P. Kubik, M. Suter, A. Mangini, A 200 kyr record of cosmogenic radionuclide production rate and geomagnetic field intensity from ^{10}Be in globally stacked deep-sea sediments, Earth Planet. Sci. Lett. 149 (1997) 121–129.
[33] R. Day, M. Fuller, V.A. Schmidt, Hysteresis properties of titanomagnetites: grain size and compositional dependence, Phys. Earth Planet. Int. 13 (1977) 260–267.
[34] W. Lowrie, Identification of ferromagnetic minerals in a rock by coercivity and unblocking temperature properties, Geophys. Res. Lett. 17 (1990) 159–162.